JOURNAL OF CATALYSIS 153, 197–207 (1995)

Methane Oxidative Coupling over Nonstoichiometric Bismuth–Tin Pyrochlore Catalysts

C. A. Mims,*[,1,2] A. J. Jacobson,† R. B. Hall,‡ and J. T. Lewandowski, Jr.‡

*Department of Chemical Engineering and Applied Chemistry, University of Toronto, Toronto, M5S 1A4; †Department of Chemistry, University of Houston, Houston, Texas 77204; and ‡Exxon Research and Engineering, Route 22E, Annandale, New Jersey 08801

Received March 1, 1994; revised January 18, 1995

A series of expanded pyrochlore oxides $Bi_2Sn_{2-x}Bi_xO_{7-x/2}$ ($0 \le x \le 0.86$) was synthesized and the influence of their composition on their performance as methane coupling catalysts was examined. A trend to higher selectivity and lower activity accompanies increases in x. However, analysis of the kinetic data by a simple procedure which separates the catalyst activity and selectivity shows that all the catalysts have similar intrinsic surface selectivities, independent of composition. The trend in observed selectivity is an indirect effect of variations in activity. The similarity in surface selectivity is attributed to the formation of a bismuth-oxide-rich surface layer in all materials upon heating to reaction temperatures. © 1995 Academic Press, Inc.

INTRODUCTION

Many oxide materials, both single and multicomponent, have been shown to be effective in the oxidative coupling of methane (1, 2). Of the binary systems, lithiated magnesia has received the most attention (3–5). The common theme among the effective catalysts is the "reducibility" of the catalyst which aids in the initial step in the reaction, the abstraction of H from methane to form methyl radicals and surface OH. The reducibility of simple systems, such as lead and manganese, arises from the multiple oxidation states of the cation. However, many other mixed metal oxides have been shown to be effective, including $LiNiO_2$ (6–8), $BaPbO_3$ (9, 10), alkaline-earth-substituted lanthanides (11–16), etc. In (Li)MgO and many of the other binary systems, substitutions in the lattice by cations of lower formal charge is thought to give rise to electrophilic (or reducible) forms of oxygen, such as O^-, which can perform the initial abstraction step.

Many mixed oxide materials may be substituted with aliovalent cations and it has been shown that pyrochlores with such substitutional defects can be synthesized (17). In some pyrochlore systems, excess A site cations substitute for some portion of the B site cations in the $A_2B_2O_7$ structure (18). The term "expanded" is applied to these materials since their lattice constants increase with increasing amounts of substitution. Stoichiometric pyrochlore oxides have received some attention as methane coupling catalysts (19–21). We have previously shown preliminary results that expanded Bi:Sn pyrochlores are effective as coupling catalysts (22, 23). The pyrochlore phases are also attractive because of their high temperature stability.

In this paper, we examine the influence of variable composition in the series $Bi_2Sn_{2-x}Bi_xO_{7-x/2}$ on the catalytic performance of these materials in the methane oxidative coupling reaction. These materials provide a well-characterized series of compounds with controlled substitutional defect concentrations. The purposes of the study are (i) to investigate this series of catalysts, and more importantly, (ii) to use the opportunity presented by a homologous series of catalysts to correlate the changes in performance with the catalyst structure. We were successful in both aims. However, in order to achieve the latter, a simple lumped kinetic analysis based on the basic methane coupling mechanism is used to separate catalyst activity and selectivity. Briefly, these two performance parameters are linked because of a difference in reaction orders between the methyl recombination reaction and methyl oxidation reactions. As shown below, by such a simple analysis, the significant trends in catalyst selectivity among the catalysts can be explained by variations in catalyst activity alone while the inherent surface selectivities remain constant.

EXPERIMENTAL

Catalyst synthesis. Table 1 lists the materials studied along with relevant characterization results. A detailed description of the synthesis of bismuth–tin pyrochlores has been given previously (22). General aspects relevant to the particular materials used as catalysts in the present

[1] E-mail: mims@ecf.toronto.edu.
[2] To whom correspondence should be addressed.

0021-9517/95 $6.00

TABLE 1

Catalyst Characterization

Sample[a,b]	Bulk composition[c]		Surface Bi/Sn ratio[d]		SA[e] (m^2/g)		Catalysis[f]
	x[g]	K/Sn	Initial	Final	Initial	Final	
1	0.23	0.010	—	—	88.7	3.2	S
2	0.26	0.310	—	—	96.4	2.2	S
3	0.66	0.000	—	—	2.2	2.0	S
4	0.71	0.030	—	—	77.6	1.4	S
5	0.80	0.020	—	—	3.1	—	S
6	0.97	0.007	—	—	48.6	—	S
7	1.20	0.043	—	—	17.9	—	S
8	0.22	0.080	—	—	93.2	24.8	S
9	0.03	0.000	—	—	2.3	2.1	S,K
10	0.06	0.090	1.0	1.2	64.9	0.9	K,S
11	0.28	0.056	—	—	58.7	0.9	K,S
12	0.56	0.053	—	—	31.7	1.0	K,S
13	0.64	0.046	1.7	2.4	58.2	1.9	S,K
14	0.80	0.020	—	—	—	0.7	K,S
15	0.85	0.006	—	—	2.5	0.9	K,S
16	0.97	0.007	—	—	48.6	0.7	K,S
17	2.00	0.000	—	—	0.7	—	K,S

[a] All samples were prepared by solution synthesis and were unsupported except for sample 9 (ceramic synthesis), sample 8 (supported on silica), and sample 17, pure Bi_2O_3 (see text).

[b] Additional samples were prepared to determine in detail the variation of lattice parameter with composition (see Fig. 1).

[c] Catalyst compositions determined by chemical analysis (Galbraith Laboratories, Knoxville, TN).

[d] XPS analysis on a Leybold–Heraus MAX 200 system, before and after heating to 650°C under vacuum.

[e] Surface areas (SA), in m^2/g, were measured on the samples as synthesized and after catalytic testing by the BET method using nitrogen sorption with an Omicron 100CX instrument.

[f] S refers to catalyst screening experiments and K to more detailed kinetic measurements as a function of gas composition and residence time.

[g] Stoichiometry parameter, x, in $Bi_2Sn_{2-x}Bi_xO_{7-x/2}$.

work are briefly summarized. Expanded pyrochlore compositions $Bi_2Sn_{2-x}Bi_xO_{7-x/2}$ ($0 \leq x \leq 0.86$) were prepared by solution syntheses. In a typical preparation, $Bi(NO_3)_3 \cdot 5H_2O$ (25 mmol, Alfa) was dissolved in 100 ml of water and 30 ml of concentrated HNO_3. Tin chloride ($SnCl_4 \cdot 5H_2O$, 25 mmol, Aldrich) was added together with 250 ml of 2 *M* KOH solution. The pH and the total solution volume were then adjusted by further addition of KOH solution. The slurry was then heated at 75–100°C for 2–5 days. The reaction product was recovered by filtration, washed, and dried at 100°C.

The specific phase and the bismuth/tin ratio in the product depend on the pH, metal ion concentration, Bi/Sn ratio, and the reaction temperature. A pure pyrochlore phase is obtained only over a narrow pH range, close to pH 13 when Bi/Sn = 1 in the initial solution. At lower pH values an amorphous phase is obtained. At higher pH a second crystalline phase (D*) is observed and becomes dominant as the pH is increased. A composition of $Bi_5Sn_2O_9(OH)_5$ was determined for D* by a combination of elemental and thermogravimetric analysis. After calcination at 400°C, X-ray diffraction showed that D* and all D*:pyrochlore mixtures convert to pure pyrochlore phases. The surface areas for pure pyrochlores formed directly from solution are typically in the range 50 to 100 m^2/g but fall to 30–50 m^2/g after calcination at 400°C. Pyrochlores obtained from D* have much lower surface areas (1–6 m^2/g).

Pure pyrochlore phase samples with different compositions were prepared by the solution synthesis method and calcined at 400°C. The compositions were determined by elemental analysis and found to fall in the range $0.05 \leq x \leq 0.86$. Samples can contain residual amounts of potassium (in the range 0.01 to 0.05 K/Bi) that is easily removed by washing with dilute acid.

Lattice parameters for the samples after calcination at 400°C were obtained by profile fitting the powder X-ray data and are shown as a function of composition in Fig. 1. The scatter in the data results from uncertainties in fitting broad diffraction peaks and possibly from inhomoge-

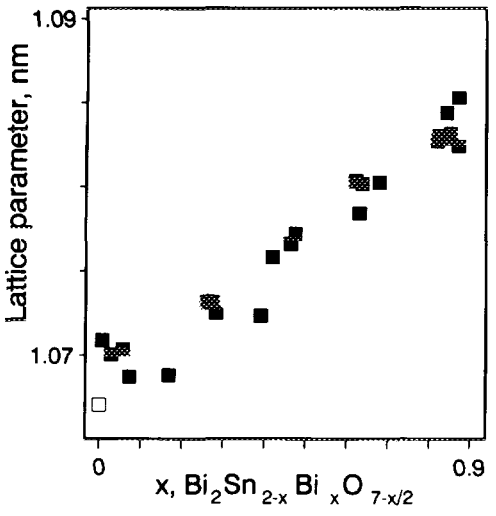

FIG. 1. Lattice parameters (unit cell volume)$^{1/3}$ in the tetragonal Bi–Sn pyrochlore unit cell versus x in $Bi_2Sn_{2-x}Bi_xO_{7-x/2}$. All catalysts from Table 1 are included.

neities in the compositions. The general increase in lattice constant with increasing composition is consistent with substitution of Bi^{3+} for Sn^{4+} and similar to data obtained for ruthenium containing pyrochlores.

The stoichiometric compound $Bi_2Sn_2O_7$ is the only stable phase at high temperature. Consequently, all of the bismuth-rich compositions are unstable and decompose when heated to temperatures above 400°C. The decomposition temperature decreases with increasing composition and varies from approximately 700°C at $x = 0.06$ (sample 10 in Table 1) to 500°C at $x = 0.85$ (sample 15). Differential thermal analysis (10°C/min to 800°C) of a sample with 0.64 (sample 13) is featureless on heating, but on cooling shows a sharp endotherm at 642°C. On reheating an exotherm is observed at 673°C and on recooling the 642°C endotherm is reproduced. These data indicate the formation of Bi_2O_3 on decomposition of the expanded pyrochlore. The presence of Bi_2O_3 and stoichiometric $Bi_2Sn_2O_7$ after heating is confirmed by X-ray diffraction. XPS measurements of the surface compositions of two catalysts show increases in the Bi/Sn ratio upon heating under vacuum (see Table 1).

Measurements of the particle size for the high surface area $Bi_2Sn_2O_7$ phases determined from the X-ray data indicate particle diameters of 5–10 nm at 400°C and 20–25 nm for samples heated to 700°C. The particle sizes determined by XRD do not reflect the true surface area because of the separation of bismuth oxide above the decomposition temperature.

Additional materials. In addition to the bismuth-rich pyrochlores, other materials were prepared for catalytic studies. Two materials with higher Bi/Sn ratios were prepared by solution techniques (samples 7 and 16), but were not single phase (Bi_2O_3 + expanded pyrochlore). A stoichiometric (Bi : Sn = 1 : 1) pyrochlore (sample 9) was prepared by high temperature ceramic methods. A stoichiometric mixture of pure Bi_2O_3 and SnO_2 powders was fused at 800°C in air, followed by repeated grinding and reheating until X-ray diffraction showed a single-phase product. A silica-supported catalyst (sample 8) was successfully prepared by solution synthesis in the presence of Cabosil. Pure Bi_2O_3 (Alfa) was also used in the catalysis studies (sample 17).

Catalysis. All materials evaluated as catalysts were pelletized, ground, and sieved to produce granular materials with 80–120 μm diameters. The reactions were carried out in a tubular quartz reactor with a 4-mm inside diameter. The catalyst temperature was monitored by a thermocouple in a 1-mm quartz sheath embedded in the catalyst charge. The reactor narrowed to 2-mm i.d. below the catalyst bed to minimize gas phase reactions in the postbed region. Methane conversions without a catalyst in the reactor were less than 1%, even at 850°C. Typically 0.25 g of catalyst rested on a shallow platform of quartz wool. The reactant gas mixtures were synthesized by mass flow controllers. The reactant gases were obtained from Matheson at stated purities of 99.99% and used without further purification.

Steady state reaction rates were measured by GC analysis of the effluent. Two types of catalytic experiments were performed. All materials were subjected to a screening protocol by stepping through a series of increasing temperatures (up to 850–900°C) with a standard gas mixture ($CH_4 : O_2 : Ar = 2 : 1 : 5$) and flow rate (80 ml (STP)/min). Multiple analyses of the reaction rate and selectivities were performed at each temperature. Following this, some or all of the same temperatures were reexamined in descending order. The bismuth oxide sample was kept below its bulk melting point of 825°C. A number of materials (noted in Table 1) were subjected to a more thorough kinetic analysis, which included variations in gas residence time and reactant gas composition. Estimates of the Thiele modulus and particle size variation assured that intraparticle mass transport limitations of the stable species were unimportant in the kinetics experiments.

Computer model. An extensive computer model of the relevant gas phase radical reactions is used briefly in this study to compare the observed kinetic behavior with that expected from gas phase pathways. This model is fully described elsewhere (24).

RESULTS AND DISCUSSION

Catalyst stability. The nonstoichiometric materials prepared by solution synthesis underwent significant

changes during their initial exposure to high temperatures. These changes include a loss of activity, a loss of surface area, and an *increase* in selectivity. Following these initial changes, the subsequent activities and selectivities were stable for periods of over 20 h at 850°C although further slow changes probably occur. Final surface areas for all materials after such treatment are near 1 m^2/g. The decrease in activity (measured at 700°C before and after higher temperature operation) was typically one order of magnitude (roughly equivalent to the decrease in surface area). Structural changes similar to those seen in thermal analysis were observed to occur after exposure to high temperature reaction conditions. X-ray diffraction shows that a mixed phase system is formed consisting of Bi_2O_3 and residual tetragonal pyrochlore with lattice parameters near those of the stoichiometric material. The silica-supported pyrochlore (sample 8) reacted partially with the support to form sillenite and SnO_2. The stoichiometric pyrochlore prepared by high temperature ceramic techniques (sample 9) on the other hand, does not deactivate, even on the first cycle. Finally, in all materials reduction of the bismuth component to metal can occur when the reactor is oxygen-starved.

Catalytic performance. These Bi–Sn pyrochlore materials show activities and selectivities comparable to the best materials so far discovered, with yields (conversion times selectivity on a carbon atom basis) of C_{2+} hydrocarbons approaching 25% (22). All rates, selectivities, and yields in this paper are reported on a C_1 basis. The reaction selectivities depend on many parameters, including catalyst composition, methane conversion, gas composition, and catalyst activity. Figure 2 shows the wide range of C_{2+} hydrocarbon selectivities observed with the standard reactant mixture for all the catalysts as a function of temperature. Only data for methane conversions of less than 15% are included in this figure. Temperatures in excess of 800°C are required to reach good levels of performance, higher than the temperatures required for catalysts such as (Li)MgO, but similar to many others (2). The reaction selectivities for all the Bi/Sn catalysts drop sharply below 800°C.

The dependence of the hydrocarbon selectivity, $S_{C_{2+}}$, on conversion and on the reactant gas composition is similar to that shown by other coupling catalysts. The data in Fig. 3, typical for all investigated, shows that the methane activation rate has positive reaction orders with respect to both methane and oxygen. The C_2 production rate responds more strongly to increases in $P(CH_4)$ than it does to $P(O_2)$ while the CO_x rate responds more strongly to increases in $P(O_2)$ than to $P(CH_4)$. As a result C_2 hydrocarbon selectivity improves with an increase in the CH_4/O_2 ratio, a common observaton for methane coupling catalysts (2). The overall effective reaction or-

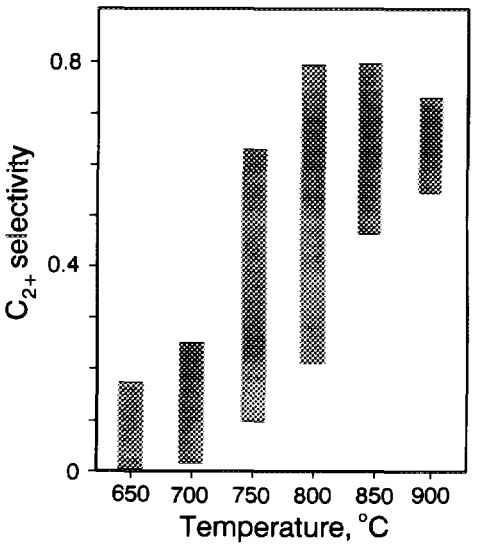

FIG. 2. Range of catalytic selectivity to C_{2+} hydrocarbons (C_1 basis) in methane oxidative coupling for the suite of Bi–Sn oxide catalysts listed in Table 1. Reaction conditions, 845°C, 100 kPa total pressure, reactant gas compositions, $CH_4 : O_2 : Ar = 2 : 1 : 5$.

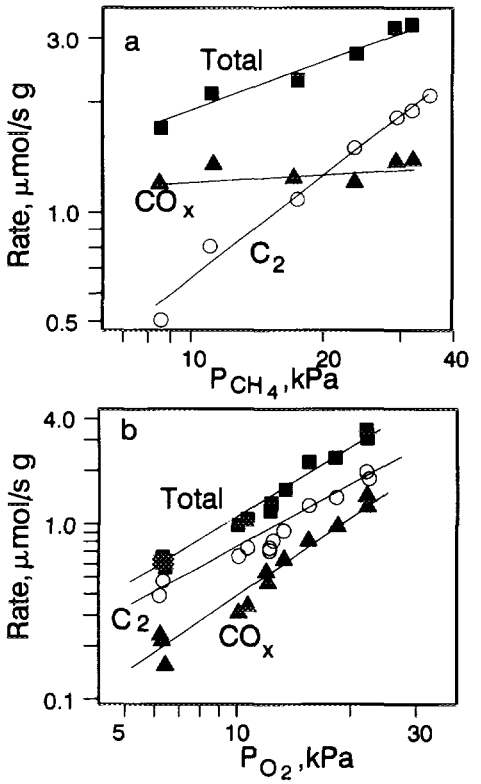

FIG. 3. Variation of catalytic production rates (C_1 basis) of C_{2+} hydrocarbons, carbon oxides and the total versus $p(CH_4)$ (a) and $p(O_2)$ (b) at 845°C over a Bi–Sn pyrochlore catalyst (sample 13 in Table 1), 100 kPa total pressure: in panel a, $p(O_2)$ = 12.5 kPa, balance Ar; in panel b, $p(CH_4)$ = 25 kPa, balance Ar.

ders are approximately 0.5 for methane and 1.0 for oxygen.

Figure 4 plots the higher hydrocarbon selectivity versus conversion achieved by variation in gas residence time. The C_{2+} selectivity seen at low methane conversions eventually decreases with increasing conversion. Higher CH_4/O_2 ratios lower the ultimate methane conversion so that the higher initial selectivity does not result in a higher yield. There have been attempts (with mixed success) to use novel reactor concepts, such as staged oxygen injection (25, 26) and chromatographic effects (27) to preserve the higher inherent selectivity at low oxygen pressures. The decrease in selectivity at high conversions could be due in part to an increase in methane or methyl radical oxidation (due, for example, to a more aggressive gas phase radical pool). However, tracer experiments on a limited number of catalysts indicate that oxidation of the C_2 products is largely responsible (24, 28–30). Another feature seen in Fig. 4 is a mild increase in selectivity to a broad maximum at intermediate conversions. This arises from complexity in the reaction rate law which is further discussed below.

The catalyst composition has an influence on activity and selectivity. Figure 5 shows the reactivity per m^2 of surface (panel a) and hydrocarbon selectivity (panel b) for various expanded pyrochlore catalysts. These data were all measured for a narrow range of methane conversions (between 15 and 20%) in the standard reactant gas mixture at 845°C and were measured during steady operation following the initial deactivation period. Of the nonstoichiometric materials, those with small values of x are the most active. Not shown is the ceramic material which does not fit this trend and has the activity of approximately 1 μmol/s · m^2. The expanded materials also show a general, if somewhat scattered, trend to higher C_{2+} selectivity with increasing bismuth content.

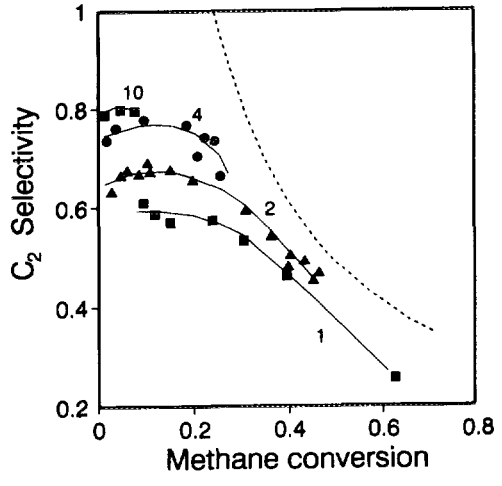

FIG. 4. Higher hydrocarbon selectivity versus methane conversion (by residence time variation) for a Bi–Sn oxide catalyst (sample 13 in Table 1) at 845 °C, 100 kPa total pressure. Reactant gas compositions, P(Ar) = 62.5 kPa; CH_4/O_2 ratios (■) = 1, (▲) = 2, (●) = 4, (■) = 10 are indicated. The dashed line is the 25% yield locus.

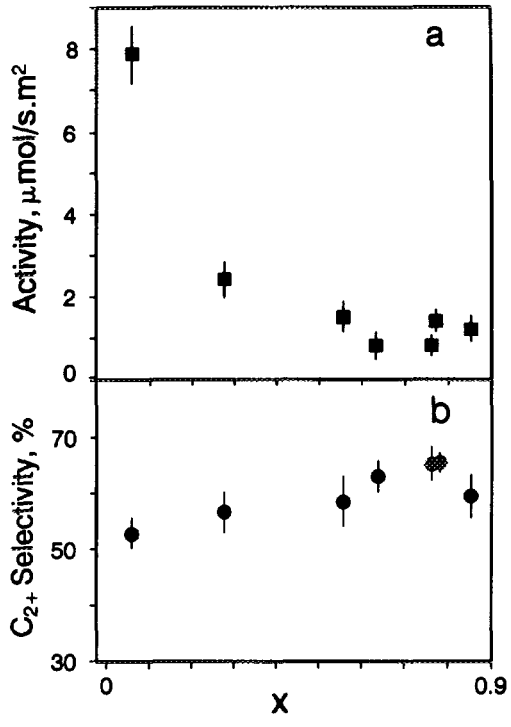

FIG. 5. Surface specific reaction rates, in μmol/s · m^2 (panel a) and $\%C_{2+}$ selectivity (panel b), both on a C_1 basis, versus x, for a series of $Bi_2Sn_{2-x}Bi_xO_{7-x/2}$ pyrochlore materials (samples 10–16 in Table 1). Data taken at 15 ± 3% methane conversion, 845°C, 100 kPa total pressure, $CH_4 : O_2 : Ar = 2 : 1 : 5$.

Kinetic analysis. In this section we correlate the trends in catalytic performance with catalyst composition. The first step requires a simple lumped kinetic analysis of the rate data to extract more fundamental information in the form of global rate coefficients from the rate data. This simple analysis, described below, removes the coupling between the catalytic activity and selectivity which arises from the reaction mechanism. The rate coefficients derived from this analysis are then used to examine the influence of catalyst composition at standard conditions, the primary aim of the study. Following this, the dependence of these rate coefficients on reaction conditions is briefly investigated.

Lumped kinetic model. There is general agreement on the basic features of the methane oxidative coupling mechanism. At low conversion, the reaction can be viewed as comprising three *global* reaction steps. First, hydrogen atom abstraction from methane by the catalyst

surface (and by gas phase radicals) produces gas phase methyl radicals

$$CH_4 \xrightarrow{k_1} CH_3. \quad [1]$$

The relative contributions of surface and gas phase processes in this step have been addressed by many groups and are probably catalyst specific. Here we describe the rate of this overall process by a volumetric (based on bed void volume) first-order rate coefficient, k_1, which itself may, of course, exhibit a complex rate law.

Much of the subsequent hydrocarbon growth chemistry is due to gas phase radical processes. The primary product hydrocarbon product, ethane, is formed by methyl radical combination in the gas phase with bimolecular rate constant k_2,

$$2CH_3 \xrightarrow{k_2} C_2H_6. \quad [2]$$

The methyl radicals can also be oxidized to form carbon oxides

$$CH_3 \xrightarrow{k_3} CO_x. \quad [3]$$

Like the methane activation step, the methyl radical oxidation rate is also described by a first-order volumetric rate coefficient, k_3, which can involve both surface and gas phase contributions. We assume that methyl oxidation is the only pathway for CO_x production from methane. These three steps can be used to describe the catalytic data as long as C_2 oxidation (or direct CH_4 oxidation) does not contribute significantly to CO_x formation. The differential C_2 selectivity (on a C_1 basis) is given by

$$S_{C2} = 1 - k_3[CH_3]/k_1[CH_4] \quad [4]$$

and by using the steady state approximation for methyl radicals

$$0 = r_{CH_3} = +k_1[CH_4] - 2k_2[CH_3]^2 - k_3[CH_3], \quad [5]$$

and substituting the resulting expression for $[CH_3]$ into [4], the expression for the hydrocarbon selectivity, S_{C2+} can be derived

$$S_{C2+} = [(1 + Y)^{1/2} - 1]/[(1 + Y)^{1/2} + 1], \quad [6]$$

where

$$Y = 8k_2k_1[CH_4]/k_3^2. \quad [7]$$

The reaction selectivity thus increases as Y increases and even in this simple version of the mechanism, the reaction selectivity is linked to catalytic activity by the fact that reaction (2) is second-order. This expression indicates that unless k_3 varies as $k_1^{1/2}$ (as some reaction parameter such as catalyst composition changes), the observed selectivity will depend on the catalyst activity, represented by k_1. Therefore, the ratio k_3/k_1 is a more fundamental measure of catalytic selectivity than is S_{C2}. Anticipating the catalytic results, it is clear from this relationship that a parallel increase in k_1 and k_3 (constant k_1/k_3) will result in a decrease in selectivity.

We now calculate values of the rate coefficients k_1 and k_3 from the catalytic data using this simple model for correlation with the catalyst composition and the reaction conditions. We limit this treatment to low conversion data, so that C_2 oxidation can be neglected and initially only consider data obtained at a single (standard) gas composition. The procedure involves three simple steps. First, k_1 is calculated from the overall methane activation rate. Then, the average methyl radical concentration in the void volume is calculated from the known (32) gas phase methyl recombination rate constant, k_2, and the C_2 formation rate. From this calculated methyl concentration, the methyl oxidation rate coefficient, k_3, can then be obtained.

The assumptions implicit in this treatment are several. The calculations require differential selectivities, whereas the experimental selectivities are integral measurements. At low conversions, we treat these as differential measurements, although, as we show later, there are minor changes over the first 10% of conversion which make even these subject to some averaging. Thus all the values for k_3 and k_1 derived from the data are weighted averages over the conversion range measured. However, the averaging is not important to the conclusions of the paper. Also implicit in this analysis is the assumption that the gas phase is locally homogeneous, i.e., that mixing is rapid compared to the reaction. In fact, there are several sources of inhomogeneity. First, the rate coefficients represent averages over the void volume of the catalyst bed and do not take into account spatial distributions of pore volume and reaction site density which could produce local variations in methyl radical density. These inhomogeneities can evolve as the catalyst desurfaces during the "run-in" period. Furthermore, even with uniform void spaces and site distribution, spatial inhomogeneities can arise due to insufficient diffusive mixing of the methyl radicals during their lifetime (33, 34). Average methyl radical lifetimes can be calculated from the reaction rate and the calculated methyl densities. These lifetimes, of the order 100 μs, are only just sufficient to diffuse a distance equal to the average particle diameter. Nonuniformities in the CH_3 concentration are therefore possible.

There is some variation in the bed void volume itself during the experiments, which has not been taken into account. Spatial inhomogeneities in reactivity may also occur simply from the variation in conversion down the bed, given the autocatalytic behavior noted above. C_2 oxidation will artificially raise the calculated value of k_3/k_1 since it decreases the calculated methyl concentration and inflates the value of k_3. Attempts to correct for this, using C_2/CH_4 oxidation rate ratios from tracer studies (24) did not appreciably affect the values of k_3/k_1 calculated below 20% methane conversion. Any inhomogeneities in composition will be magnified if channeling and/or other deviations from plug flow exist. Finally, postbed homogeneous reactions can also have a significant impact (35). Since the postbed volume in the heated zone was held to a minimum, we do not believe that such effects are present here. Keeping these complicating effects in mind, we now use this procedure to analyze the catalytic results.

Trends with catalyst composition. The calcualted values of k_3/k_1 for catalysts 9–17 at two different temperatures and under standard reaction conditions are shown in Fig. 6. The values at 845°C are restricted to a narrow conversion range, thus limiting any averaging effects. The 700°C data represent a wider conversion range (2 to 10%) and are somewhat more scattered, but values for pure bismuth oxide are also available at this temperature.

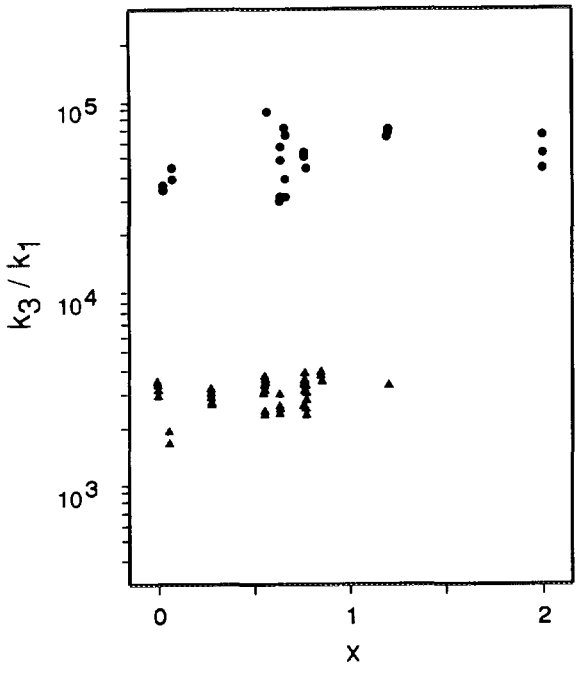

FIG. 6. Dependence of the rate coefficient ratio k_3/k_1 on x in $Bi_2Sn_{2-x}Bi_xO_{7-x/2}$ pyrochlore materials (samples 9–17 in Table 1). Methane conversions <20%, 100 kPa total pressure, $CH_4:O_2:Ar = 2:1:5$; 700 ± 5°C (●); 845 ± 5°C (▲).

Even with the scatter, it is clear that the average values of k_3/k_1 show no visible trend with composition, including Bi_2O_3. Therefore, according to this analysis, the catalysts here appear to differ from one another largely with respect to volumetric activity and, since the surface areas are similar for the expanded pyrochlores, surface activity. They *do not*, however, show a significant variation in inherent selectivity in this analysis. The higher k_3k_1 ratios at 700°C than at 845°C reflect a higher activation energy for k_1 than for k_3.

Similar surface chemistry among the catalysts is a logical explanation for the uniform values of k_3/k_1. A bismuth-rich oxide surface layer is consistent with the structural changes and the XPS results, even for the stoichiometric pyrochlores. The fact that the ratio k_3/k_1 for Bi_2O_3 is similar to that of the pyrochlores is especially convincing. Therefore, what appears to be a trend to higher selectivity in Fig. 5 with increasing Bi/Sn ratios is an indirect result of a trend to lower activity and not a result of changes in the inherent surface selectivity of the materials.

Changes upon annealing. The expanded pyrochlores lose activity and gain selectivity as a result of the initial exposure to high temperature reaction conditions. Figure 7 shows these changes for one of the catalysts (sample 13) during the initial screening experiment. The deactivation during the first heating cycle is clearly shown in the activation rate coefficient, k_1 in panel 7a. Arrhenius behavior is seen on the descending temperature sequence but the final rate at 700°C is 1/10th its initial value. As panel 7b shows, the hydrocarbon selectivity at 700°C is improved after this high temperature excursion. The values of k_3 (Fig. 7c) also show an irreversible change. While k_1 after annealing has a strong temperature dependence (205 kJ/mol), the methyl oxidation rate coefficient, k_3, has a weaker non-Arrhenius temperature dependence. The ratio k_3/k_1 decreases with increasing temperature, as shown in panel d and similar to the findings in the previous section. The significant finding is that the value of this ratio at 700°C remains almost unchanged despite the 10-fold decrease in activity during this experiment. The change in selectivity can be attributed solely to desurfacing of the catalyst while the surface selectivity remains unchanged. Therefore, most of the change in selectivity seen in this annealing experiment is consistent with that predicted by Eqs. [6] and [7] as a byproduct of the decrease in k_1.

It is interesting at this point to compare trends in selectivity predicted by a gas phase radical mechanism with these catalytic results. A gas phase mechanism might also be expected to produce parallel trends in k_1 and k_3. Figure 8 provides a comparison of the dependences of the C_2 selectivity on volumetric activity, represented by the

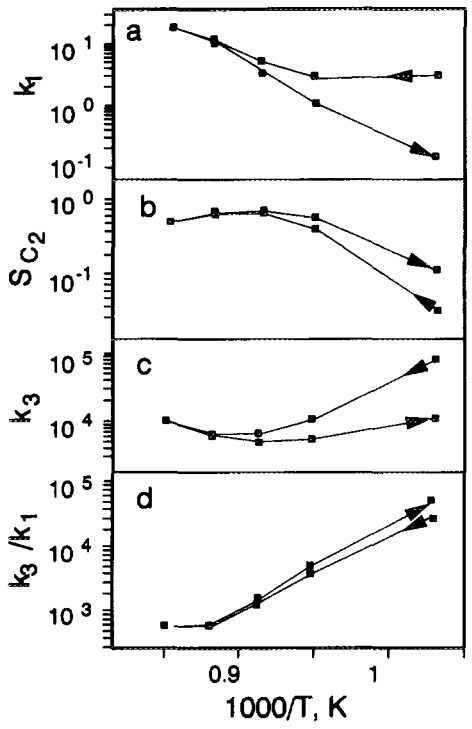

FIG. 7. Arrhenius plots of the variation of the rate coefficients and selectivity with temperature for $Bi_2Sn_{2-x}Bi_xO_{7-x/2}$ (sample 13 in Table 1) during initial screening cycle (see text); (a) k_1, s^{-1}; (b) C_{2+} selectivity; (c) k_3 (s^{-1}); and (d) k_3/k_1 during initial screening (see text). The total pressure was 100 kPa; $CH_4:O_2:Ar = 2:1:5$. Arrows show temporal order of experiments.

global rate coefficient, k_1, for (i) the experimental data, (ii) the simple lumped model with constant k_3/k_1 and (iii) the predictions of a computer model of the gas phase chemistry. The catalytic selectivity data at two temperatures (700 and 845°C) at standard gas composition are included for all the catalysts in Table 1. The data set includes all methane conversions between 0.05 and 0.2, and oxygen conversions of less than 0.4. Minor additional scatter is produced by including a somewhat wider range of conditions. For constant k_3/k_1 the selectivity is a single-valued function of the catalytic activity, k_1. The dashed lines in Fig. 8 are the predictions of Eq. [6] using the best values of k_3/k_1 (constant at each temperature) from Fig. 6. There is scatter in the data, but the obvious trend in the data is well represented by this prediction.

A gas phase radical mechanism (initiated by the catalyst surface) would have the opposite trend in selectivity with catalyst activity to that seen in the data. The solid lines in Fig. 8 show the predictions of a gas phase reaction model in which the only catalytic step is methyl production. The computer model is similar to other published model (36–41) and contains 175 reactions involving C_1 and C_2 species (24). A series of simulations with a range of assumed activation rates produced the solid lines in Fig. 8. The calculated selectivities are higher than observed, especially at 700°C. More significantly, the trends are opposite to the experimental data. The calculations are indicative of the selectivity of an unperturbed gas phase mechanism since the model predicts two to five methane molecules to be activated by the gas phase radical pool for every one activated on the surface. In order for the selectivity to increase with activity, the value of k_3/k_1 calculated by the model must decrease markedly with activation rate. The results above argue against the dominance of gas phase radical reactions in determining k_3.

Effect of gas composition. A brief examination of the trends in k_1 and k_3 with gas composition is instructive, and although the data are not extensive enough for a full kinetic study, they illustrate some of the averaging in the simple analysis and provide further mechanistic insight. The data in Fig. 9, taken at constant low (0.03) conversion, show the effects of methane and oxygen partial pressure on k_1, k_3, and k_3/k_1. In panel a, methyl oxidation, k_3, is shown to be unaffected by changes in CH_4 partial pressure. On the other hand, k_1 shows a negative order in $p(CH_4)$ which simply reflects the fact that the overall rate, given by $k_1[CH_4]$, is less than first-order in methane. Again, k_1 represents the global activation pro-

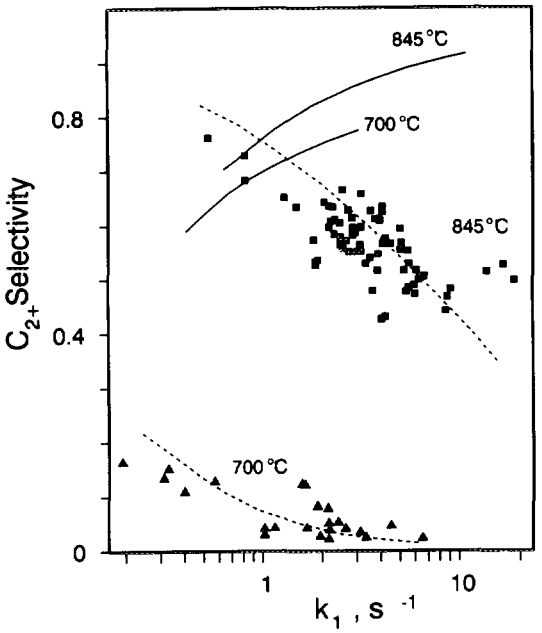

FIG. 8. C_{2+} selectivity versus k_1: data points are from all $Bi_2Sn_{2-x}Bi_xO_{7-x/2}$ catalysts listed in Table 1, at 845 ± 5°C (■) or 700 ± 5°C (▲) with methane conversion <20%. The dashed curves are selectivities calculated by Eqs. [6] and [7] with: k_3/k_1 (700°C) = 3.6×10^4 and k_3/k_1 (845°C) = 4.0×10^3. The solid lines are simulated results (15% methane conversion) using a gas phase reaction model described in the text.

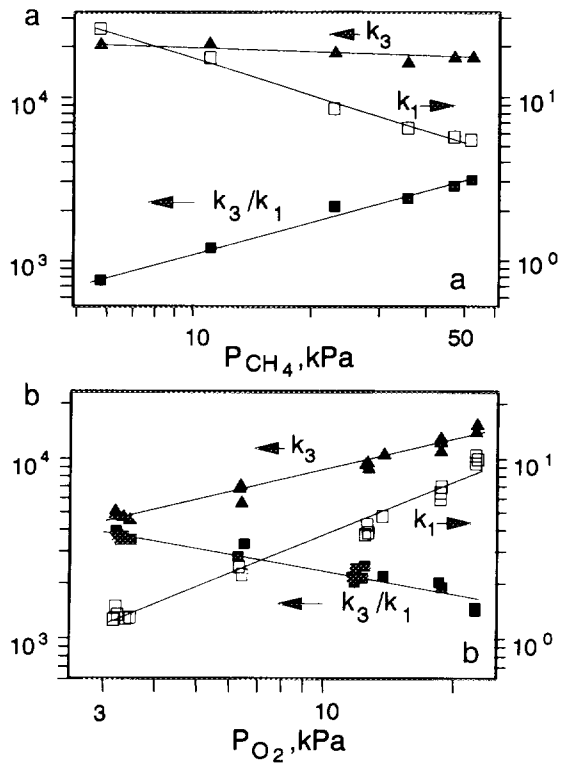

FIG. 9. Variation of the rate coefficients with methane partial pressure (panel a) and oxygen partial pressure (panel b): Data measured at 845°C at 100 kPa total pressure on catalyst 13; $p(CH_4)$ = 25 kPa (panel a) and $p(O_2)$ = 12.5 kPa (panel b), balance Ar. Units of k_1 and k_3 are s^{-1}.

cess, both gas phase and surface and could even represent a first-order surface activation process followed by a radical chain length which declines with methane pressure. Computer model calculations suggests that the chain length would decrease with methane pressure, but because of unknown heterogenous reaction steps, any quantitative comparisons based on those calculations are not warranted. Both k_1 and k_3 have similar dependence on oxygen partial pressure (Fig. 9b) so that the ratio, k_3/k_1, is relatively constant. With constant k_3/k_1, the increase in activity with increasing $p(O_2)$ causes a decrease in selectivity (see Eq. [6] and Fig. 3).

The global rate coefficients also show a mild dependence on conversion, even at low conversion, which reflects the influence of the products on the reaction rates. It adds to the amount of averaging associated with the foregoing analysis. Figure 10 shows k_1 and k_3 values derived from a residence time study. Both k_1 and k_3 decrease moderately with conversion but k_3 shows a somewhat stronger variation, so that a modest decrease in k_3/k_1 occurs over this conversion range. Because of the averaging in the k_3/k_1 values calculated, the actual trends with conversion are somewhat more pronounced. The combination of decreasing activity and decreasing k_3/k_1 with conversion produces the mild maximum in integral selectivity seen in Fig. 4 over the 0–20% conversion range. Similar effects were noted on other catalysts, and the resulting k_3/k_1 ratios at a given conversion were quite similar although there are substantial variations in volumetric activity. The residual differences in k_3/k_1 after annealing (Fig. 7) can be attributed to the resulting change in conversion. The source of the conversion dependence is the effect of accumulating products, particularly H_2O and CO_2, on the surface processes. Additionally, contributions by the gas phase pathways may augment either process. This is plausible as the buildup of C_2 products in the gas phase will increase the radical chain length (24, 36–38).

General discussion. The lumped kinetic analysis was critical in unifying an apparently erratic dependence of reaction selectivities on catalyst structure. The surface selectivities of these catalysts do not show any discernible variation with the catalyst composition, suggesting that the catalytic surface in all cases is a Bi_2O_3-rich film. In this regard, bismuth oxide is a good coupling catalyst and can selectively couple propene to form 1,5-hexadiene (42, 43). The catalysts exhibit variability in activity per unit surface area, so that a simple model of a Bi_2O_3 surface film does not provide a complete picture. However, even this conclusion must be taken with caution, since

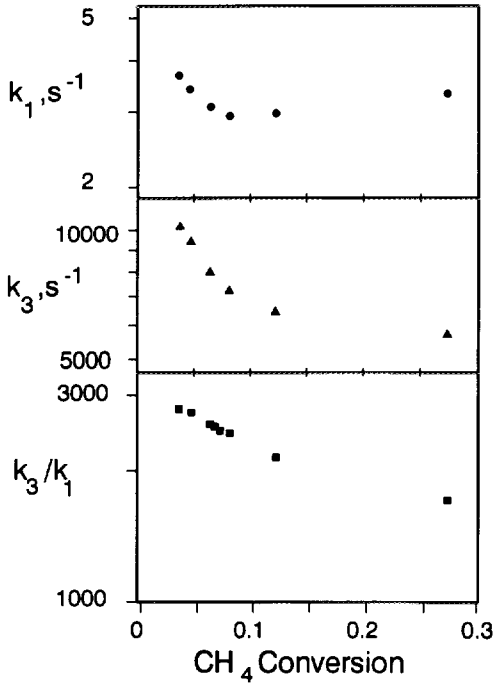

FIG. 10. Variation of rate coefficients k_1 (in s^{-1}), k_3 (In s^{-1}) and the ratio k_3/k_1 as a function of methane conversion on catalyst 13. 100 kPa total pressure, $CH_4:O_2:Ar$ = 2:1:5, 845°C.

the surface areas at reaction conditions may differ substantially from those measured after reaction. Residual substitutions in the lattice or surface layer may have an effect on oxygen mobility, or other processes related to restoration of the abstraction site and therefore surface activity. Finally, the storage of a surface active component in solid state solution may be important in maintaining the desired surface composition in this and other systems. In any case, the role of defects is hidden by the phase separation which is observed.

Several findings point to a dominance of surface reactions in the oxidation of methyl radicals. First, the computer model predicts a gas-phase-dominated reaction to increase in selectivity as activity increases, rather than to decrease as seen experimentally. The constant k_3/k_1 ratio (conversion effects excluded) is seen over a wide range of catalysts and conditions. Surface reactions for both processes involving a common surface intermediate would naturally exhibit such behavior. Also consistent with surface reactions are the observed dependences of k_1 and k_3 on gas phase composition. Both the absence of a methane pressure dependence on k_3 and similar oxygen pressure dependences for k_1 or k_3 are consistent with surface processes, but not characteristic of gas phase reactions. Finally, support for the dominance of surface processes in deep oxidation has come from isotope tracer studies of competitive CH_4/C_2 oxidation (24, 27–31) on other catalysts, comparative rate measurements (44), and studies of kinetic isotope effects (45). The gas phase model predicts that addition of C_2 hydrocarbons to the CH_4/O_2 reactant should increase the production of CO_x from methyl. This effect arises from the formation of HO_2 and other aggressive radicals as a result of C_2 oxidation processes. As a result of these processes, the model predicts the C_2 selectivity to degrade rapidly with conversion, more rapidly than is seen experimentally. Experimentally, however, C_2 addition does not produce an increase in C_1 oxidation but merely increases CO_x production by oxidation of C_2. There is strong evidence that surface processes interfere with the gas phase radical pool (24, 46, 47). The destruction of peroxy species (which are key gas phase chain carriers and methyl oxidizers) is particularly important. The direct measurement of the CH_3 surface oxidation rate for these catalysts as has been done for others would provide a direct test of this interpretation.

ACKNOWLEDGMENTS

We thank Richard Haverkamp and Fazila Seker for obtaining XPS information, G. Stuhne for the model calculations, E. B. Sirota for the synchrotron X-ray data and S. L. Soled for the DTA measurements. Support by the Natural Sciences and Engineering Research Council of Canada, Exxon and Imperial Oil, Ltd. (CAM), and by the R. A. Welch Foundation (AJJ) is gratefully acknowledged.

REFERENCES

1. Wolf, E. E., (Ed.), "Methane Conversion by Oxidative Processes", van Nostrand–Reinhold, New York, 1992 contains many contributions which review the current status of various aspects of methane coupling.
2. Amenomiya, Y., Birss, V. I., Goledzinowski, M., Galuszka, J., and Sanger, A. R., *Catal. Rev. Sci. Eng.* **32,** 163 (1990).
3. Ito, T., and Lunsford, J. H., *Nature* **314,** 721 (1985).
4. Ito, T., Want, J. X., Lin, C. H., and Lunsford, J.H., *J. Am. Chem. Soc.* **107,** 5062 (1985).
5. Driscoll, D. J., Martir, W., Wang, J. X., and Lunsford,J. H., *J. Am. Chem. Soc.* **107,** 58 (1985).
6. Hatano, M., and Otsuka, K., *Inorg. Chim. Acta* **146,** 243 (1988).
7. Hatano, M., and Otsuka, K., *J. Chem. Soc. Faraday Trans. I* **85,** 199 (1989).
8. Pickering, I. J., Maddox, P. J., and Thomas, J. M., *Chem. Mater.* **4,** 994 (1992).
9. Dissanayake, D., Kharas, K. C. C., Lunsford, J. H., and Rosynek, M. P., *J. Catal.* **139,** 652 (1993).
10. Kharas, K. C. C., and Lunsford, J. H., *J. Am. Chem. Soc.*, 2336 (1989).
11. Machida, K., and Enyo, M., *J. Chem. Soc. Chem. Commun.*, 1639 (1987).
12. Zhang, Z. L., and Baerns, M., *J. Catal.* **135,** 317 (1991).
13. Washecheck, D. M., *et al.*, U.S. Patent 5196634 1993.
14. Xu, Y. D., Yu, L., Huang, J. S., and Lin, Z. Y., *Stud. Surf. Sci. Catal.*, **75,** 2209 (1993).
15. Yamashita, H., Machida, Y., and Tomita, A., *Appl. Catal. A: General* **79,** 203 (1991).
16. Kalenik, Z., and Wolf, E. E., *Stud. Surf. Sci. Catal.* **75,** 1093 (1993).
17. Subramanian, M., Aravamudan, G., and Subba Rao, G. V., *Prog. Solid State Chem.* **15,** 55 (1983).
18. Horowitz, H. S., Longo, J. M., and Lewandowski, J. T., *Mater. Res. Bull.* **1F6,** 489 (1981). Horowitz, H. S., Longo, J. M., Horowitz, H. H., and Lewandowski, J. T., *ACS Symp. Ser.* (R. K. Grasselli, & J. F. Bradzil, Eds.), **279,** 143 (1985).
19. Ross, J. A., Bakker, A. G., Bosch, H., van Ommen, J. G., and Ross, J. R. H., *Catal. Today* **1,** 133 (1987).
20. Ashcroft, A. T., Cheetham, A. K., Green, M. L. H., Grey, C. P., and Vernon, P. D. F., *J. Chem. Soc. Chem. Commun.* 1667 (1989).
21. Petit, C., Kaddouri, A., Libs, S., Kiennemann, A., Rehspringer, J. L., and Poix, P., *J. Catal.* **140,** 328 (1993).
22. Jacobson, A. J., Lewandowski, J. T., Mims, C. A., Hall, R. B., and Meyers, G. R., *NIST Spec. Pub.* **804,** 151 (1991).
23. Mims, C. A., Hall, R. B., Jacobson, A. J., Lewandowski, J. T., and Myers, G., *ACS Symp. Ser.* **482,** 230 (1992).
24. Mims, C. A., Mauti, R., Dean, A. M., and Rose, K. D., *J. Phys. Chem.* **98,** 13,357 (1994).
25. Santamaria, J., Menedez, M., Pena, J. A., and Barahona, J. I., *Catal. Today* **13,** 353 (1992).
26. Ekstrom, A., *in* "Methane Conversion by Oxidative Processes" (E. E. Wolf, Ed.), p. 99. van Nostrand–Reinhold, 1992.
27. Tonkovich, A. L., Carr, R. W., and Aris, R., *Science* **262,** 221 (1993).
28. Ekstrom, A., and Lapszewicz, J. A., *J. Phys. Chem.* **93,** 5230 (1989).
29. Nelson, P. F., and Cant, N. W., *J. Phys. Chem.* **94,** 3756 (1990).
30. Shamsi, A., *Ind. Eng. Chem. Res.* **32,** 1877 (1993).
31. Papageorgiou, D., Vamvouka, D., Verykios, X. E., *Stud. Surf. Sci. Catal.* **75** (New Frontiers in Catalysis, Pt. C), 2269 (1993).
32. Tsang, W., *J. Phys. Chem. Ref. Data* **17,** 887 (1988); **16,** 471 (1987).

33. Reyes, S. C., Kelkar, C. P., and Iglesia, E., *Catal. Lett.* **19,** 167 (1993).
34. Reyes, S. C., Iglesia, E., Kelkar, C. P., *Chem. Eng. Sci.* **20,** 48 (1993).
35. van Kasteren, H. M. N., Geerts, J. W. M. H., and van der Wiele, K. *in* "Proceedings, 9th International Congress on Catalysis, Calgary, 1988" (M. J. Phillips and M. Ternan, Eds.), Vol. 2, p. 930. Chem. Institute of Canada, Ottawa, 1988.
36. Mackie, J. C., Smith, J. G., Nelson, P. F., and Tyler, R. J., *Energy Fuels* **4,** 277 (1990).
37. McCarty, J. G., McEwen, A. B., and Quinlan, M. A., *in* "New Developments in Selective Oxidation" (G. Centi, and F. Trifiro, Eds.), Elsevier, Amsterdam, 1990.
38. McCarty, J. G. *in* "Methane Conversion by Oxidative Processes" (E. E. Wolf, Ed.), van Nostrand–Reinhold, New York, 1992.
39. Geerts, W. M. H., Chen, Q., van Kasteren, J. M. N., and van der Wiele, K., *Catal. Today 6*, 519 (1990).
40. Zanthoff, H. W., and Baerns, M. *Ind. Eng. Chem. Res.* **29,** 2 (1990).
41. Zhu, J. Y., Dittmeyer, R., and Hofmann, H., *Chem. Eng. Process.* **32,** 167 (1993).
42. Haber, J., and Grzybowska, B., *J. Catal.* **28,** 489 (1983).
43. Solymosi, F., and Bozso, F., *in* "Proceedings, 6th International Congress on Catalysis, London, 1976" (G. C. Bond, P. B. Wells, and F. C. Tompkins, Eds.), Vol. 1, p. 365. The Chemical Society, London, 1977.
44. Roos, J. A., Korf, S. J., Veehof, R. H. J., van Ommen, J. G., and Ross, J. R. H., *Appl. Catal.* **52,** 147 (1989).
45. Shi, C. L., Xu, M. T., Rosynek, M. P., and Lunsford, J. H., *J. Phys. Chem.* **97,** 216 (1993).
46. Hatano, M., Hinson, P. G., Vines, K. S., and Lunsford, J. H., *J. Catal.* **124,** 557 (1990).
47. Sinev, M. Yu., Vorobieva, G. A., and Korchak, V. N., *Kinet. Katal.* **27,** 1164 (1986).